Stochastic electron motion in colliding plane waves

A. R. Knyazev ⬤ and S. I. Krasheninnikov
University of California San Diego, La Jolla, California 92093-0411, USA

The stochastic dynamics of an electron in counterpropagating linearly polarized laser beams is analyzed using a recently developed 3/2-dimensional Hamiltonian approach. It is shown that perpendicular canonical momenta suppress stochasticity, helping to explain the results from recently reported numerical studies of stochastic dynamics in a similar setting. The stochasticity in a perpendicular polarization setup is demonstrated. Lastly, the impact of radiation friction effects is considered, and shown to be negligible in the classical radiation reaction limit.

I. INTRODUCTION

The stochastic dynamics of electrons interacting with multiple electromagnetic waves has been studied using the Hamiltonian formalism [1,2] and investigated via numerical simulations [3–6]. Recently, a novel approach [7] was proposed, where the dynamics of the relativistic electron in two collinearly polarized counterpropagating plane waves was described with a 3/2-dimensional (3/2D) Hamiltonian, allowing one to apply the techniques used in previous studies of stochastic dynamics in such systems [8,9]. However, the effects of perpendicular canonical momenta $\mathbf{P}_\perp$ of the electron were not considered in the previous analysis of stochasticity. Considering these effects enables a better understanding of the recent numerical results of stochastic heating in colliding laser pulses, such as the dependence on the initial laser phases [5].

In this paper, we expand on a previous stochastic motion analysis [7] to account for perpendicular canonical momenta $\mathbf{P}_\perp$, and allow for an arbitrary angle between linear polarizations of two counterpropagating waves. We discuss the effect of $\mathbf{P}_\perp$ on stochastic heating, and relate that effect to the impact of the initial laser phases. Finally, we consider stochastic heating in the presence of radiation friction.

II. STOCHASTIC MOTION

To provide context for the present discussion, it is instructive to revisit the well-known problem of the interaction between a single electron in vacuum with the laser pulse described by a vector potential $\mathbf{a_1} = a_1 \sin(\eta)\mathbf{e_x}$, where $\eta = t - z$, $a_1 = eE_1/mc\omega$ is the normalized amplitude of the vector potential, E_1 is the maximum electric field of the laser, λ is the laser wavelength, c is the speed of light in vacuum, and m and $-e$ are the electron's mass and charge, respectively. In what follows, we use dimensionless units, normalized by the introduced constants as follows: The length is normalized by $k = 2\pi/\lambda$, time by ω, the electron's velocity $\mathbf{v}$ and canonical momenta $\mathbf{P}$ by c and mc, respectively, and the electric and magnetic fields by $e/mc\omega$. The outlined problem has three

well-known integrals of motion,

$$\gamma - P_z = H = \text{const}, \quad P_{x,y} = \text{const}, \tag{1}$$

where $P_{x,y,z}$ are components of $\mathbf{P} = \gamma\mathbf{v} - \mathbf{A}$, γ is the Lorentz factor of the electron, and $\mathbf{A}$ is the vector potential of the electric $-\partial_t \mathbf{A}$ and magnetic $\nabla \times \mathbf{A}$ field. In the reference setup $\mathbf{A}$ equals simply $\mathbf{a_1}$. The expression for the Lorentz factor of the electron follows from the integrals of motion in Eqs. (1),

$$\gamma = \frac{1}{2}\left(H + \frac{\mathcal{E}_p}{H}\right), \tag{2}$$

where $\mathcal{E}_p = 1 + (P_x + A_x)^2 + (P_y + A_y)^2$. In the rest of the paper, we will refer to the maximum of Eq. (2) as ponderomotive scaling γ_p. Now, consider that a second laser was added to the setup, described by $\mathbf{a_2} = a_2 \sin(k_2\tau)(\alpha\mathbf{e_x} + \sqrt{1-\alpha^2}\mathbf{e_y})$, where $\tau = t + z$, k_2 is the wave number of the second laser, and α is the cosine of the angle between $\mathbf{a_1}$ and $\mathbf{a_2}$. The introduction of $\mathbf{a_2}$ breaks the conservation of H, and it was shown that even $a_2 \ll a_1$ can enhance the maximum Lorentz factor γ. Significant physical insight into this phenomenon was obtained by using a 3/2-dimensional Hamiltonian description [7] of the electron dynamics in colliding laser beams, where it was shown that the role of the perturbation laser $\mathbf{a_2}$ is to cause the onset of stochasticity in H, with the stochastic change in H then leading to an increase of electron energy γ_p. A performed analysis of stochasticity [7] was, however, limited to the case of parallel pulse polarization with both lasers propagating along the general momenta of the electron, $P_\perp = 0$. In this section, we will generalize the analysis of stochastic heating to the case of $P_\perp \neq 0$. We show that both $P_x \gg a_1$ and $P_y \gg a_1$ suppress stochasticity. For cases where stochasticity is still present, we show that $P_y > 0$ and $P_x \gtrsim a_1$ increase the lower stochastic limit $H_{\min}$, while keeping the higher stochastic limit $H_{\max}$ intact. Based on the $H_{\min/\max}$ limits, we explain how $|P_x|$ and $|P_y|$ affect the limits of stochastic heating relative to the ponderomotive scaling $\max(\gamma_s)/\mathcal{E}_p$, where γ_s is the ponderomotive scaling Eq. (2) for the initial value of the dephasing
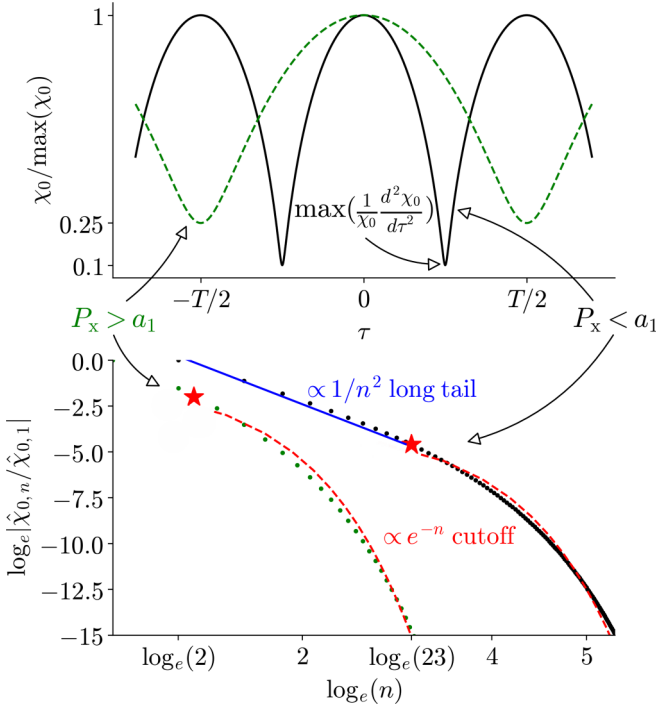
FIG. 1. Top panel: Unperturbed trajectories $\chi_0(\tau)$ for $P_x < a_1$ ($P_x = 0$, $P_y = 0$, $a_1 = 3.0$ for the black solid curve), and for $P_x > a_1$ ($P_x = 15$, $P_y = 0$, $a_1 = 5.0$ for the green dashed curve). Bottom panel: Corresponding magnitudes of normalized harmonics $|\hat{\chi}_{0,n}|$ for $P_x > a_1$ (curve on the left), and for $P_x < a_1$ (curve on the right). The blue solid line shows the long tail of Fourier harmonics, and the red dashed curves show the exponential decay of harmonic amplitudes. Red stars show the exponential cutoff estimates (10) and (11)

rate H_0. We verify our analysis with a series of Poincaré maps obtained from a numerical integration of Eqs. (3)–(5) below.

We begin by describing the dynamics of the electron interacting with both laser beams $\mathbf{A} = \mathbf{a}_1 + \mathbf{a}_2$ as a 3/2D Hamiltonian [7] system,

$$H = \frac{1}{\chi}\{1 + [P_x + a_1 \sin(\eta) + \alpha a_2 \sin(k_2\tau)]^2$$

$$+ [P_y + \sqrt{1-\alpha^2} a_2 \sin(k_2\tau)]^2\} = \gamma - P_z, \quad (3)$$

$$\frac{d\eta}{d\tau} \equiv \dot{\eta} = -\frac{\partial H}{\partial \chi} = \frac{H}{\chi}, \quad (4)$$

$$\frac{d\chi}{d\tau} \equiv \dot{\chi} = \frac{\partial H}{\partial \eta} = \frac{2a_1\cos(\eta)[P_x + a_1\sin(\eta)]}{\chi}, \quad (5)$$

where $\chi = \gamma + P_z$. Because the onset of stochasticity is typically attributed to the overlap of high harmonic resonances [8], it is instructive to begin the analysis with the study of the Fourier harmonics $\hat{\chi}_0(\Omega)$ of unperturbed ($a_2 = 0$) $\chi_0(\tau)$ electron motion, and analyze how the spectrum depends on $P_{x,y}$. As Fig. 1 illustrates, unperturbed electron motion $\chi_0(\tau)$ is a nonlinear periodic oscillation with a base frequency Ω, and so the Fourier spectrum consists of discrete harmonics $\hat{\chi}_{0,n}$, where n is the harmonic's number. A typical $\hat{\chi}_0(\Omega)$ spectrum has a tail of Fourier harmonics with a power-law amplitude decay $|\hat{\chi}_{0,n}| \propto 1/n^2$, followed by an exponential cutoff $|\hat{\chi}_{0,n}| \propto \exp[-(n - n_c)]$, where n_c is the cutoff

harmonic number,

$$n_c^2 = \frac{\Omega_c^2}{\Omega^2} \approx \frac{1}{\Omega^2} \max\left(\frac{1}{\chi}\frac{d^2\chi}{d\tau^2}\right). \quad (6)$$

The cutoff frequency $\Omega_c \approx \max(\ddot{\chi}_0/\chi_0)$ corresponds to the most rugged parts of $\chi_0(\tau)$. Unless $P_x \approx a_1$, $\max(\ddot{\chi}_0/\chi_0)$ occurs at minima $\min(\chi_0) \equiv \chi_m$ along the unperturbed trajectory, so we can estimate the cutoff frequency as

$$\Omega_c^2 = \frac{1}{\chi}\frac{d^2\chi}{d\tau^2}\bigg|_{\chi_m} = 2a_1 H^4$$

$$\times \frac{a_1\cos^2(\eta_m) - \sin(\eta_m)[P_x + a_1\sin(\eta_m)]}{\left\{1 + P_y^2 + [P_x + a_1\sin(\eta_m)]^2\right\}^3}, \quad (7)$$

where η_m is the value of η corresponding to χ_m. It follows from the Hamiltonian Eq. (3) that $\sin(\eta_m) = -a_1/P_x$ for $|P_x| < a_1$, and $\sin(\eta_m) = -P_x/|P_x|$ otherwise. We can use Eqs. (6) and (7) to determine the number of unsuppressed Fourier harmonics n_c by comparing Ω_c with the frequency of unperturbed motion Ω. To find Ω, we solve for implicit $\eta_0(\tau)$ dependence,

$$\tau + \text{const} = \frac{1}{H^2}\left[\left(1 + P_x^2 + P_y^2 + \frac{a_1^2}{2}\right)\eta_0 \right.$$

$$\left. -2a_1 P_x\cos(\eta_0) - \frac{a_1^2}{4}\sin(2\eta_0)\right], \quad (8)$$

and calculate the unperturbed frequency as

$$\Omega = \frac{2\pi}{\tau(\eta_0 + 2\pi) - \tau(\eta_0)} = \frac{H^2}{1 + P_x^2 + P_y^2 + a_1^2/2}. \quad (9)$$

Combining Eq. (6) with results from Eqs. (7) and (9) gives

$$n_c^2 = \frac{2a_1\left(1 + P_x^2 + P_y^2 + a_1^2/2\right)^2(|P_x| - a_1)}{\left[1 + P_y^2 + (|P_x| - a_1)^2\right]^3} \quad (10)$$

for the $|P_x| \gg a_1$ case, and

$$n_c^2 = \frac{2\left(1 + P_x^2 + P_y^2 + a_1^2/2\right)^2\left(a_1^2 - P_x^2\right)}{\left(1 + P_y^2\right)^3} \quad (11)$$

in the $|P_x| \ll a_1$ case. Estimates (10) and (11) agree with the Fourier transforms $\hat{\chi}_0$ shown in Fig. 1, where the sharp corners in the $P_x \ll a_1$ case result in a long tail of harmonics, while the $P_x \gg a_1$ case has a virtually instantaneous exponential cutoff of its spectrum. It follows from Eqs. (10) and (11) that both $|P_x| \gg a_1$ and $|P_y| \gg a_1$ result in a low-frequency cutoff $\Omega_c \approx \Omega$ and therefore suppress stochasticity. However, for moderate values of $|P_x|$ and $|P_y|$, there exists a long tail of unsuppressed Fourier harmonics in the spectrum of unperturbed motion. From Chirikov's stochasticity criterion, this long tail in the spectrum allows for island overlap and results in a wider stochastic region [8].

Our next step is to determine how components of canonical momenta $P_\perp$ affect the stochasticity boundaries $H_{\max/\min}$. For an electron with an initial Hamiltonian H_0, Eq. (2) predicts that an increased stochastic region will subsequently lead to further heating for cases where the stochastic limits $H_{\max} > \mathcal{E}_p$ or $H_{\min} < 1$. To find the $H_{\max/\min}$ limits, we note that the
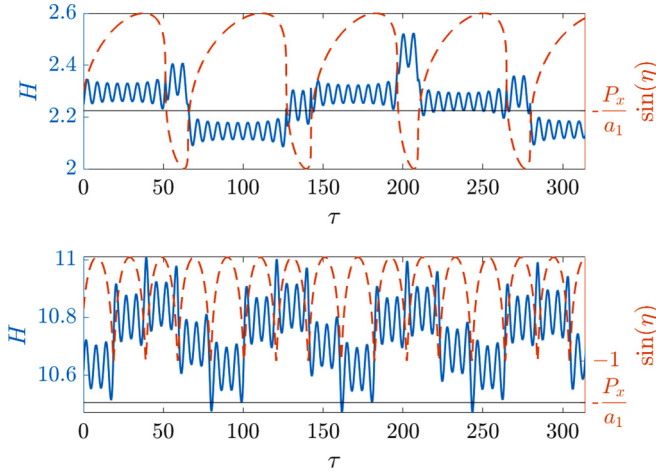
FIG. 2. Hamiltonian H (solid blue curves) and $\sin(\eta)$ (dashed orange curves) for $a_1 = 10$, $a_2 = 0.1$, $k_2 = 1$. The top panel shows the case with $P_x/a_1 \approx 0.25$, where "kicks" occur at $\sin(\eta) = -a_1/P_x$. The bottom panel shows the case with $P_x/a_1 = 1.8$, where "kicks" occur at $\sin(\eta) = -P_x/|P_x| = -1$.

evolution of the Hamiltonian,

$$\frac{dH}{d\tau} = \frac{2a_2 k_2 \cos(k_2 \tau)}{\chi}[\alpha P_x + \sqrt{1 - \alpha^2} P_y \\ + \alpha a_1 \sin(\eta) + a_2 \sin(k_2 \tau)], \tag{12}$$

is adiabatic outside of regions with minimal χ. If the second laser $\mathbf{a}_2$ is a perturbation $a_2 \ll a_1$, from Eqs. (3) and (12) it follows that the value of H changes during "kicks" at

$\sin(\eta) = -a_1/P_x$ for $P_x < a_1$ and $\sin(\eta) = -P_x/|P_x|$ otherwise, as illustrated in Fig. 2. The change in H during one kick is

$$\Delta H_n = \int \frac{dH}{d\tau} d\tau = \int \frac{\chi}{H} \frac{dH}{d\tau} d\eta, \tag{13}$$

and the difference in the phase of $\mathbf{a}_2$ between two consecutive kicks is

$$\Delta\psi_n = \frac{2\pi k_2}{\Omega_{n+1}} = \frac{2\pi k_2}{H_{n+1}^2}\left(1 + P_x^2 + P_y^2 + \frac{a_1^2}{2}\right), \tag{14}$$

if $|P_x| > a_1$, and

$$\Delta\psi_n = \frac{[\pi \pm 2\arcsin(P_x/a_1)]k_2}{H_{n+1}^2}\left(1 + P_x^2 + P_y^2 + \frac{a_1^2}{2}\right), \tag{15}$$

otherwise. The sequence of kicks described by (13)–(15) will lead to stochasticity if [8]

$$K \equiv \left|\frac{d\Delta\psi_n}{dH_{n+1}}\frac{d\Delta H_n}{d\psi_n}\right| \gtrsim 1. \tag{16}$$

From Eq. (16), we can obtain the limits of stochasticity $H_{\max/\min}$, and the corresponding maximum electron energy (2). Details of the calculation are outlined in Eqs. (17)–(20) below, followed by the resulting expressions for the stochastic boundaries.

As discussed above, the motion outside the kick regions can be approximated as adiabatic, allowing us to substitute the unperturbed trajectory Eq. (8) into Eq. (12) for evaluating the integral in Eq. (13). For kicks in the $|P_x| < a_1$ regime, the outlined substitution yields

$$k_2\tau = \tilde{\phi} + \frac{k_2}{H^2}\left(\left[1 + P_x^2 + P_y^2 + \frac{a_1^2}{2}\right]\eta - 2P_x^2 \sin(\eta) - 2P_x\sqrt{a_1^2 - P_x^2}\cos(\eta) + \left(\frac{P_x^2}{2} - \frac{a_1^2}{4}\sin(2\eta)\right) + \frac{1}{2}P_x\sqrt{a_1^2 - P_x^2}\cos(2\eta)\right), \tag{17}$$

where

$$\tilde{\phi} = \text{const} - \frac{k_2}{H^2}\left(1 + P_x^2 + P_y^2 + \frac{a_1^2}{2}\right)\arcsin\left(\frac{P_x}{a_1}\right). \tag{18}$$

Note that in the stochastic regime where H exhibits random behavior, the $\tilde{\phi}$ also becomes random. To simplify the notation below, we combine $\tilde{\phi}$ with all other constants independent of η. We can now approximate the trajectory around the kick with a Taylor expansion of Eq. (17) at $\sin(\eta_m) = -P_x/a_1$, allowing for the following approximation for integrals in (13):

$$\int_{\tau_{\text{kick}}} \cos(k_2\tau)d\eta = \int_{-\infty}^{\infty}\cos\left(\tilde{\phi} + \frac{k_2}{H^2}(1 + P_y^2)\eta + \frac{1}{3}(a_1^2 - P_x^2)\eta^3 + P_x\sqrt{a_1^2 - P_x^2}\eta^4 - \frac{1}{60}(4a_1^2 - 7P_x^2)\eta^5\right)d\eta. \tag{19}$$

The phase of cosine terms in the integral in Eq. (19) varies rapidly away from the $\eta = 0$ point, and so for an asymptotic analysis is suffices to keep the lowest nonlinear term (η^3 for $P_x < a_1$ and η^5 for $P_x = a_1$).

The analysis done in Eqs. (17)–(19) can be repeated for $P_x \gtrsim a_1$, where kicks occur at $\sin(\eta_m) = -P_x/|P_x|$, and the resulting approximations for integrals in Eq. (13) are different from Eq. (19):

$$\int_{\tau_{\text{kick}}} \cos(k_2\tau)d\eta = \int_{-\infty}^{\infty}\cos\left(\tilde{\phi} + \frac{k_2}{H^2}[1 + P_y^2 + (P_x - a_1)^2]\eta + \frac{a_1}{3}(P_x - a_1)\eta^3 - \frac{a_1}{60}(4a_1 - P_x)\eta^5\right)d\eta. \tag{20}$$

For even larger $P_x \gg a_1$ values, the kick approximation is no longer valid, and the motion is not stochastic, in agreement with the analysis of the trajectory Fourier spectrum in Eq. (10).

Note that in the Hamiltonian description, the phase trajectory explicitly depends only on $\mathbf{P}_\perp$ and the initial conditions $\eta(\tau_0)$, $\chi(\tau_0)$, and does not depend on the initial phases ϕ_1 and ϕ_2 of the lasers. In a previous study of the interaction between the multipicosecond laser and the overdense plasma target [5], the stochastic electron dynamics of the electron in the presence of incident and reflected laser pulses was numerically simulated using noncanonical variables $\gamma\mathbf{v}$, $a_1 \sin(\phi_1)$, $a_2 \sin(\phi_2)$ to describe

the electron dynamics, resulting in the appearance of laser phases ϕ_1 and ϕ_2 in the final answer. The use of canonical variables χ and η (η corresponding to the "phase slip" from Ref. [5]) enables us to understand the physics of the stochasticity onset, illustrating that stochasticity is impacted by canonical momenta $\mathbf{P}_\perp$ rather than the laser phases.

Equipped with approximations (19) and (20), we can now evaluate the integral Eq. (13) in the $P_x < a_1$, $P_x = a_1$, and $P_x > a_1$ regimes, and assess the impact of P_x and P_y on the stochastic boundaries $H_{\max/\min}$. For moderate values of $P_x < a_1$, "kicks" correspond to $\sin(\eta_m) = -P_x/a_1$, giving the stochasticity condition

$$\left| 8\pi a_2 \left(\sqrt{1-\alpha^2} \frac{a_1^{5/3}|P_y|\beta^{5/2}}{(a_1^2 - P_x^2)^{1/3}} \mathrm{Ai}\left[\frac{a_1^{2/3}(1+P_y^2)\beta}{(a_1^2 - P_x^2)^{1/3}} \right] - \alpha \frac{a_1^{4/3}\beta^2}{(a_1^2 - P_x^2)^{1/6}} \mathrm{Ai}'\left[\frac{a_1^{2/3}(1+P_y^2)\beta}{(a_1^2 - P_x^2)^{1/3}} \right] \right.\right.$$
$$\left.\left. + \frac{a_1^{5/3}a_2\beta^{5/2}}{2^{1/3}(a_1^2 - P_x^2)^{1/3}} \mathrm{Ai}\left[\frac{(2a_1)^{2/3}(1+P_y^2)\beta}{(a_1^2 - P_x^2)^{1/3}} \right] \right) \left(1 + P_x^2 + P_y^2 + \frac{a_1^2}{2}\right) \left[\pi \pm 2\arcsin\left(\frac{P_x}{a_1}\right)\right] \right| \gtrless 1, \tag{21}$$

where we introduced the parameter $\beta = (k_2/a_1 H^2)^{2/3}$. For $P_x \gtrsim a_1$, the stochasticity condition is

$$\left| \frac{8\pi^2 a_1^{4/3} a_2 \beta^{5/2}}{(P_x - a_1)^{1/3}} \left([\alpha(P_x - a_1) + \sqrt{1-\alpha^2}P_y]\mathrm{Ai}\left[\frac{(1+(P_x-a_1)^2+P_y^2)a_1^{1/3}\beta}{(P_x - a_1)^{1/3}} \right] \right.\right.$$
$$\left.\left. + \frac{a_2}{2^{1/3}} \mathrm{Ai}\left[\frac{(1+(P_x-a_1)^2+P_y^2)(4a_1)^{1/3}\beta}{(P_x - a_1)^{1/3}} \right] \right) \left(1 + P_x^2 + P_y^2 + \frac{a_1^2}{2}\right) \right| \gtrless 1. \tag{22}$$

To compare Eqs. (21) and (22) with results obtained from numerically integrating Eqs. (3)–(5), we calculated the Poincaré maps of the electron's dynamics in lasers with various a_1, a_2, k_2, and α, for various initial H and $\mathbf{P}_\perp$. The resulting Poincaré maps (see Fig. 3, for example) allow us to estimate the stochastic boundary $\beta_{\max/\min}$ since

$$H_{\min/\max} = \sqrt{k_2/a_1 \beta_{\max/\min}^{3/2}}. \tag{23}$$

Figure 4 demonstrates the agreement between estimates from Eqs. (21) and (22) and numerical simulations with initial $\beta = (0.1)^{2/3}$. Despite preserved Kolmogorov-Arnol'd-Moser (KAM) surfaces (such as the smooth curve on the top and island in Fig. 3) preventing the precise measurement of the stochastic boundary in some simulations, the results shown in
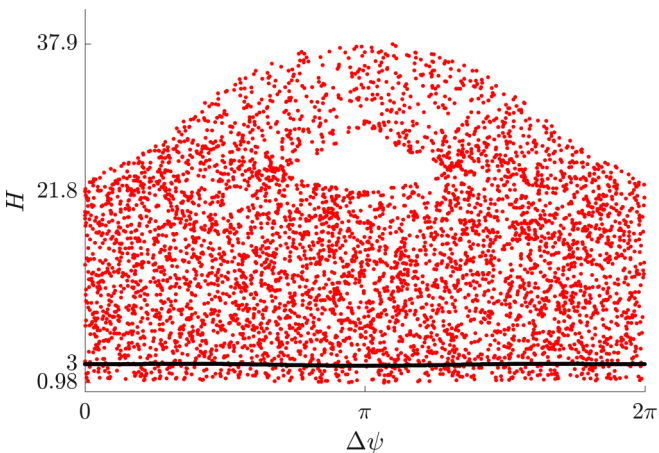
Fig. 4 show good agreement of the numerical results with the analysis.

From the estimates in Eqs. (21) and (22), and given the asymptotics of the Airy function [$\mathrm{Ai}(x) \sim 0.36 - 0.26x$ for $x \to 0$ and $\mathrm{Ai}(x) \sim 0.28x^{1/4}\exp(-2x^{3/2}/3)$ for $x \to \infty$], it follows that the stochastic region $\beta_{\max} - \beta_{\min}$ is maximized for $P_\perp = 0$. Both $\beta_{\max}$ and $\beta_{\min}$ decrease with the growth of
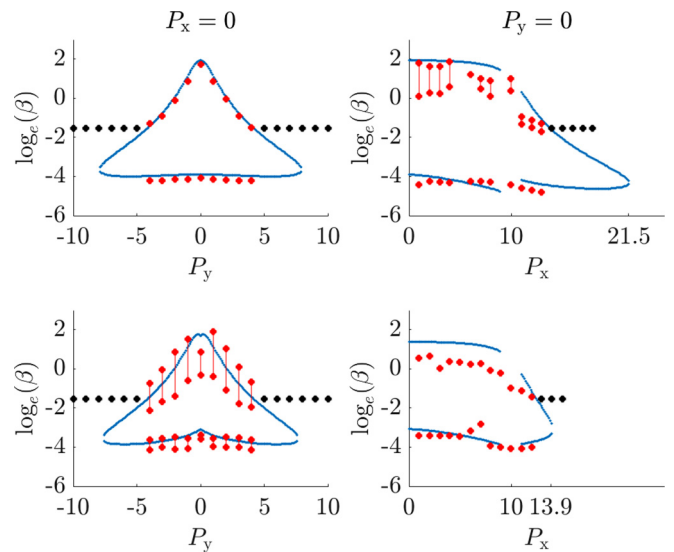

FIG. 4. Stochastic boundary Eqs. (21) and (22) for $K = 5$, plotted with blue lines for laser amplitudes $a_1 = 10$, $a_2 = 1$, in the cases of parallel ($\alpha = 1$, top panels) and perpendicular ($\alpha = 0$, bottom panels) polarizations. Electrons have either $P_x = 0$ or $P_y = 0$ on the left and right panels, respectively. Red dots show the stochastic boundary from the series of Poincaré simulations with initial $\beta = (0.1)^{2/3}$, $\eta(0) = 0$, and $k_2 = 9$ or 1089 (the use of larger values of k_2 allows for a more precise measurement of β from the Poincaré maps in some simulations, since the stochastic region remains in $H > 1$). Black dots mark simulations with no stochasticity.

FIG. 3. Poincaré cross sections for an electron with initial $H(0) = 3$, $\eta(0) = 0$, and $\mathbf{P}_\perp = P_y\mathbf{e}_y$ from a setup with the parameters $a_1 = 10$, $a_2 = 1$, $k_2 = 9$, $\alpha = 1$. The red dots show stochastic motion for $P_y = 2$, and the black line at $H = 3$ shows regular motion for $P_y = 5$.
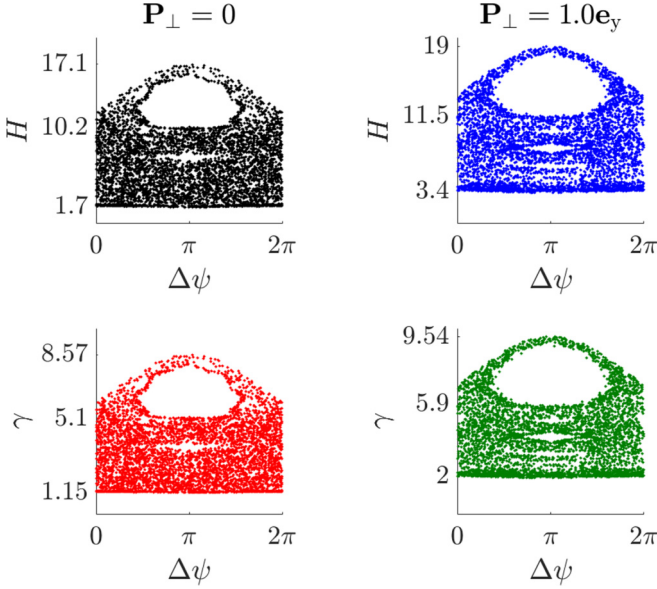
FIG. 5. Poincaré cross sections for $\alpha = 1$, $a_1 = 2$, $a_2 = 0.1$, $k_2 = 50$, $\mathbf{P}_\perp = 0$ (left panels), and $\mathbf{P}_\perp = 1.0\mathbf{e}_y$ (right panels). The corresponding ponderomotive energies $\gamma_p \approx 2.4$ ($\mathbf{P}_\perp = 0$) and 2.6 ($\mathbf{P}_\perp = 1.0\mathbf{e}_y$).

$|P_\perp|$, however, the β_{min} boundary is much less sensitive to both P_x and P_y. From Eq. (23) we then conclude that H_{max} decreases with $|P_\perp|$, while H_{min} remains intact. At large $|P_\perp|$ it follows from Eqs. (21) and (22) that stochasticity becomes completely suppressed, in agreement with the spectral analysis above.

Because H_{min} increases with P_y^2, stochastic energy is suppressed if its maximum $\max(\gamma_s)$ corresponds to $H_{min} < 1$. However, if $\max(\gamma_s)$ corresponds to $H_{max} > \mathcal{E}_p$, the efficiency of stochastic heating $\max(\gamma_s)/\mathcal{E}_p$ remains the same with an increase of P_y. $H_{max} > \mathcal{E}_p$ requires large k_2,

$$k_2 > \left[1 + (P_x + A_x)^2 + (P_y + A_y)^2 \right] a_1 \beta_{min}^{3/2}, \quad (24)$$

as in the simulation shown in Fig. 5.

The analysis above demonstrated that large $|\mathbf{P}_\perp| \gg a_1$ suppresses stochastic heating. For larger amplitudes of the main laser $\mathbf{a}_1$, the perpendicular canonical momentum will no longer be conserved due to radiation friction effects. To see how radiation friction (RF) affects the stochastic heating, we use the classical Landau and Lifshitz [10] approximation for RF force,

$$\mathbf{f} = \rho_f \{ -\gamma^2 \mathbf{v} [(\mathbf{E} + \mathbf{v} \times \mathbf{B})^2 - (\mathbf{v} \cdot \mathbf{E})^2]$$
$$+ \gamma [(\partial_t + \mathbf{v} \cdot \nabla)\mathbf{E} + \mathbf{v} \times (\partial_t + \mathbf{v} \cdot \nabla)\mathbf{B}]$$
$$+ [\mathbf{E} \times \mathbf{B} + \mathbf{B} \times (\mathbf{B} \times \mathbf{v}) + \mathbf{E}(\mathbf{v} \cdot \mathbf{E})] \}, \quad (25)$$

where $\mathbf{E} = -\partial_t \mathbf{a}_1$, $\mathbf{B} = \nabla \times \mathbf{a}_1$, $\rho_f = 2kr_e/3$, and $r_e = e^2/mc^2 \approx 2.8$ fm is the classical radius of the electron. Estimating $\gamma \sim a_1^2$, $\mathbf{E} \sim a_1$, it follows from Eq. (25) that the RF force is comparable to the Lorentz force when $\rho_f a_1^5 \sim 1$. For lasers with a wavelength of about 0.5 μm, the $\rho_f a_1^5 \sim 1$ condition is satisfied for $a_1 \gtrsim 40$. Substituting $\mathbf{a}_1 = a_1 \sin(\eta)$ into Eq. (25) gives the expression

$$\mathbf{f} = \rho_f \{ a_1 H (1 - v_z) \sin(\eta)\mathbf{e}_x - \mathbf{v} a_1^2 H^2 \cos^2(\eta)$$
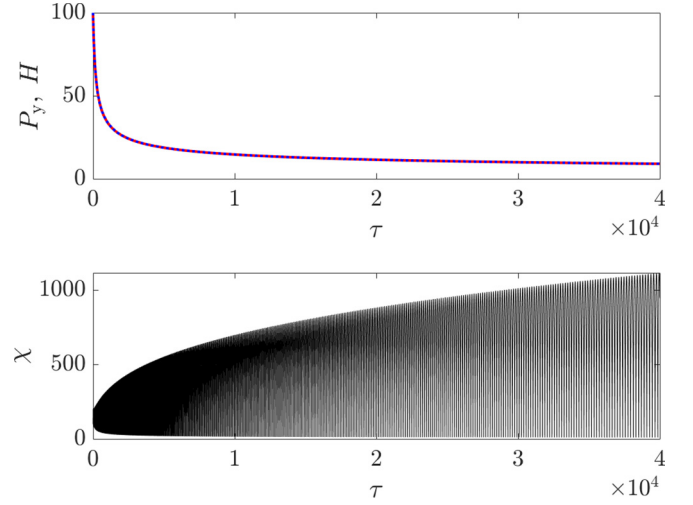$$+ a_1 H v_x \sin(\eta)\mathbf{e}_z + a_1^2 (1 - v_z) \cos^2(\eta)\mathbf{e}_z \}, \quad (26)$$

FIG. 6. Top panel: Decay of $P_\perp(\tau)$ and H caused by radiation friction for $\lambda = 1$ μm, $a_1 = 100$, and initial $\mathbf{P}_\perp = 100\mathbf{e}_y$. Bottom panel: Corresponding evolution on $\chi(\tau)$.

that we combine with the equations of motion for the electron,

$$\frac{d\mathbf{P}}{d\tau} = \frac{\gamma}{\chi}\mathbf{f}. \quad (27)$$

The $\mathbf{P}_\perp$ components of (27) are

$$\frac{dP_x}{d\tau} = -\frac{\rho_f a_1^2 H^2}{\chi} \left([P_x + A_x] \cos^2(\eta) - \frac{\sin(\eta)}{a_1} \right), \quad (28)$$

$$\frac{dP_y}{d\tau} = -\frac{\rho_f a_1^2 H^2}{\chi} [P_y + A_y] \cos^2(\eta), \quad (29)$$

where $A_{x,y}$ are components of $\mathbf{A} = \mathbf{a}_1 + \mathbf{a}_2$. The evolution of χ is described by

$$\frac{d\chi}{d\tau} = \frac{\partial H}{\partial \eta} + \frac{\gamma}{\chi}(\mathbf{v} \cdot \mathbf{f} + f_z). \quad (30)$$

Using Eq. (26), expression (30) can be rewritten as

$$\frac{d\chi}{d\tau} = \frac{\partial H}{\partial \eta} + \frac{H + \chi}{2\chi} \rho_f \{ a_1^2 \cos^2(\eta)$$
$$\times [1 - v_z^2 - H^2(v_z + \mathbf{v}^2)] + 2a_1 H v_x \sin(\eta) \}, \quad (31)$$

where the velocity components can be expressed as

$$v_{x,y} = \frac{2(P_{x,y} + A_{x,y})}{\chi + H}, \quad v_z = \frac{\chi - H}{\chi + H}. \quad (32)$$

Finally, Eq. (4) does not change in the presence of RF, since

$$\frac{d\eta}{d\tau} = \frac{1 - v_z}{1 + v_z} = \frac{\gamma - p_z}{\gamma + p_z} = \frac{H}{\chi} = -\frac{\partial H}{\partial \chi}. \quad (33)$$

It follows from Eqs. (28) and (29) that $|P_\perp| > a_1$ converges to $P_x \sim a_1$ and $P_y \sim \sqrt{1 - \alpha^2} a_2$. For electrons with an initial $P_\perp = 0$, the period of electron motion $T = 2\pi/\Omega \sim a_1^2$, and, since $\chi = \gamma + P_z \sim a_1^2$, from Eq. (28) it follows that $P_x(T) \sim \rho_f a_1^3$. Since for lasers with a micron wavelength $\rho_f \sim 10^{-8}$, it follows that P_x and P_y will remain zero for laser amplitudes $a_0 \ll 10^3$, consistent [11] with the classical approximation from Ref. [10] given by Eq. (25). Since $\rho_f H^2 \ll \Omega$ for $P_\perp \lesssim a_0$ values, the dynamics described by Eqs. (28) and (29) are

much slower than the characteristic period of electron motion (as illustrated in Fig. 6), and so the analysis of stochastic heating performed for taking $P_\perp$ constant remains valid.

III. CONCLUSION

In this paper, we described stochastic heating of an electron with anarbitrary canonical momentum $\mathbf{P}$ in the presence of two counterpropagating linear plane waves with an arbitrary angle between the polarization. We demonstrated that the onset of stochasticity is possible for both parallel and perpendicular polarization setups. For the $a_2 \ll a_1$ case, we derived the stochasticity threshold and showed how the stochastic region of H decreases with an increase of perpendicular canonical momenta $\mathbf{P}_\perp$. We demonstrated that for $|\mathbf{P}_\perp| \ll a_1$, the Fourier spectrum of unperturbed $a_2 = 0$ electron motion

has a long tail of harmonics with a power-law amplitude decay $|\hat{\chi}_{0,n}| \propto 1/n^2$, allowing for a resonant overlap and the onset of stochasticity, in agreement with the Chirikov criterion. [8] Meanwhile, in the $|\mathbf{P}_\perp| \gg a_1$ case, the exponential cutoff in the Fourier spectrum $|\hat{\chi}_{0,n}| \propto \exp(-n)$ prevents the onset of stochasticity. The presented results reveal the physics behind the impact of $\mathbf{P}_\perp$ on the stochasticity boundary. Finally, we expanded the Hamiltonian analysis to include the impact of radiation friction in the classical radiation reaction limit. We demonstrated that within the applicability of classical approximation from Ref. [10], the impact of $P_\perp$ is much slower than the period of electron motion, and the Hamiltonian analysis $P_\perp = $ const for stochastic heating remains valid.

The presented results are useful for understanding the electron dynamics in counterpropagating laser pulses such as, for example, the incident-reflected laser pulses in laser-target interactions [5,6,12].

[1] J. T. Mendonca, Phys. Rev. A **28**, 3592 (1983).

[2] J.-M. Rax, Phys. Fluids B **4**, 3962 (1992).

[3] Z.-M. Sheng, K. Mima, Y. Sentoku, M. S. Jovanović, T. Taguchi, J. Zhang, and J. Meyer-ter-Vehn, Phys. Rev. Lett. **88**, 055004 (2002).

[4] S. Bochkarev, E. d'Humières, V. Tikhonchuk, P. Korneev, and V. Y. Bychenkov, Plasma Phys. Controlled Fusion **61**, 025015 (2019).

[5] K. Weichman, A. P. Robinson, F. N. Beg, and A. V. Arefiev, Phys. Plasmas **27**, 013106 (2020).

[6] A. Kemp and S. Wilks, Phys. Plasmas **27**, 103106 (2020).

[7] Y. Zhang and S. Krasheninnikov, Phys. Plasmas **26**, 050702 (2019).

[8] R. Z. Sagdeev, D. A. Usikov, and G. M. Zaslavsky, *Nonlinear Physics: From the Pendulum to Turbulence and Chaos* (Harwood Academic, New York, 1988).

[9] A. J. Lichtenberg and M. A. Lieberman, *Regular and Stochastic Motion*, Vol. 38 (Springer, Berlin, 2013).

[10] L. D. Landau, *The Classical Theory of Fields*, Vol. 2 (Elsevier, Amsterdam, 2013).

[11] T. Nakamura, Phys. Rev. E **102**, 033210 (2020).

[12] B. S. Paradkar, M. S. Wei, T. Yabuuchi, R. B. Stephens, M. G. Haines, S. I. Krasheninnikov, and F. N. Beg, Phys. Rev. E **83**, 046401 (2011).